Inwardly Rotating Spiral Waves in a Reaction-Diffusion System

Vladimir K. Vanag and Irving R. Epstein*

Almost 30 years have passed since the discovery of concentric (target) and spiral waves in the spatially extended Belousov-Zhabotinsky (BZ) reaction. Since then, rotating spirals and target waves have been observed in a variety of physical, chemical, and biological reaction-diffusion systems. All of these waves propagate out from the spiral center or pacemaker. We report observations of inwardly rotating spirals found in the BZ system dispersed in water droplets of a water-in-oil microemulsion. These "antispirals" were also generated in computer simulations.

Outwardly rotating spiral waves (spirals) (*1*) or concentric waves (pacemakers) (*2*) are vivid and ubiquitous phenomena in reaction-diffusion systems. Spirals are observed in nonlinear homogeneous chemical systems (*1*, *3*–*6*), in heterogeneous catalytic reactions on crystal surfaces (*7*), and in a variety of biological systems, e.g., in cardiac muscle (*8*–*10*), in insect population dynamics (*11*), during intracellular Ca^{2+} release from *Xenopus laevis* oocytes (*12*), and during aggregation of *Dictyostelium discoideum* amoebae (*13*). Usually, spirals emerge in an excitable (or oscillatory) medium as the result of a wave break. Open ends of a broken wave evolve because of the dependence of the normal wave velocity, $v(r)$, on the curvature, $1/r$, according to the eikonal equation (*14*, *15*)

$$v(r) = c_0 - D/r \qquad (1)$$

where c_0, which is unique for a given medium, is the velocity of a plane wave and D is the diffusion coefficient of an excitable species (activator) that stimulates its own production in an autocatalytic reaction. The local curvature near the open wave ends is high, making the velocity of the end small and forcing it to rotate around the spiral core. The limiting velocity c_0 is given by a dispersion relation that relates the wave velocity to the wavelength and is of the order of $(\gamma D)^{1/2}$, where γ is the rate of autocatalysis. Some systems contain two activator species with very different diffusion coefficients (*16*) or reaction rates (*17*, *18*). In such systems, the characterization of c_0 and the validity of Eq. 1 are not so evident, and new patterns may emerge.

Our work deals with the spatially extended oscillatory BZ reaction in water-in-oil AOT microemulsion (BZ-AOT system) (*16*, *19*, *20*). This system consists of nanometer-sized water droplets dispersed in a continuous oil (octane) phase. Each droplet is surrounded by a surfactant monolayer. The surfactant in our system is sodium bis(2-ethylhexyl)-sulfosuccinate, known as Aerosol OT (AOT) (*21*). The BZ reagents, which are polar, are dissolved initially in the aqueous phase, i.e., in the water droplets. When the BZ reaction starts, bromine and the autocatalytic species $BrO_2^{\bullet}$, which are nonpolar, are produced in the water droplets and can diffuse into the oil phase. Communication between droplets may occur through the oil phase via fast diffusion of these small molecules ($BrO_2^{\bullet}$ and Br_2) or as a result of mass exchange during droplet collision/fusion/fission.

Nonlinear systems in microheterogeneous media offer an attractive subject for investigation, because they are better analogs of living systems than are the more commonly studied nonlinear reactions in homogeneous media. In some sense, the BZ-AOT system is similar to that of a population of microorganisms. Droplets inject small signaling molecules into the continuous phase, as do motile chemotactic cells of *Escherichia coli*, which excrete the attractant aspartate (*22*), or of the slime mold *D. discoideum*, which produce cyclic adenosine monophosphate (cAMP) (*13*). Patterns observed during the development of *D. discoideum* and *E. coli* colonies are strongly dependent on the concentration of cells (*13*, *22*). A similar behavior is observed in the BZ-AOT system, where at the same chemical composition, Turing structures are found at low (<0.5) volume fraction of droplets, ϕ_d, standing waves at intermediate (0.5 to 0.7) ϕ_d, and accelerating waves at higher values (*16*).

We studied the oscillatory BZ-AOT system far from the boundary between the reduced steady state and oscillatory state of the BZ-AOT stirred system. At the chosen reactant concentrations, there is a critical value of the droplet fraction, ϕ_{cr}, above which a sudden substantial increase in frequency and decrease in amplitude of oscillations occur in a stirred BZ-AOT system (*20*). The spatially extended BZ-AOT system demonstrates a marked change in behavior in passing through ϕ_{cr}. Our experiment was performed as follows. Two stock microemulsions with the same size and concentration of water droplets were prepared by mixing for several hours a 1.5 M solution of AOT in octane with an aqueous solution of either H_2SO_4 and malonic acid or ferroin and $NaBrO_3$ ($\phi_d = 0.71$). To obtain microemulsions with different ϕ_d, we diluted the stock microemulsions with octane. The reaction was initiated by mixing the two stock microemulsions. A small volume of the reactive BZ-AOT microemulsion was sandwiched between two flat optical windows. The gap between the windows was determined by the thickness h (= 0.1 mm) of an annular Teflon gasket with inner and outer diameters of 20 and 47 mm, respectively. Patterns were observed at 23°C for about 1 hour through a microscope equipped with a digital charge-coupled device camera connected to a personal computer.

At $\phi_d < \phi_{cr}$, outward (ordinary) spiral waves were found. At $\phi_d > \phi_{cr}$, we observed inwardly rotating spirals (Fig. 1, A to C) as well as inwardly moving circular waves (Fig. 1D). These "antispirals" and "antipacemakers" may coexist simultaneously in different regions of the microemulsion layer. Which object arises at a given position apparently depends on the initial conditions. Two-armed

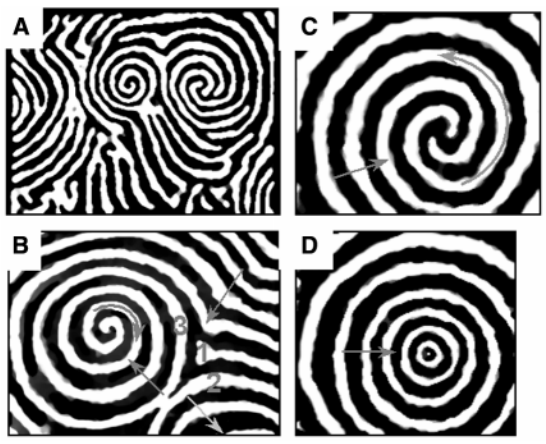

Fig. 1. Fully developed inwardly moving spiral and target patterns in BZ-AOT microemulsion. (**A** to **C**) Antispirals, $\phi_d = 0.55$. (**D**) Concentric waves (antipacemaker), $\phi_d = 0.59$. For all microemulsions, $\omega \equiv [H_2O]/[AOT] = 15$, $[MA]_0 = 0.3$ M, $[H_2SO_4]_0 = 0.2$ M, $[ferroin]_0 = 4$ mM. $[NaBrO_3]_0$ (in M) = 0.23 (A), = 0.2 [(B) and (C)], and 0.21 (D). Frame size (in millimeters): (A) 5.1 by 3.75, (B) 3 by 2.25, (C) 1.8 by 1.5, and (D) 2.7 by 2.5. Arrows mark directions of wave movement and antispiral rotation.

Department of Chemistry and Volen Center for Complex Systems, Brandeis University, Waltham, MA 02454, USA.

*To whom correspondence should be addressed. E-mail: epstein@brandeis.edu

(Fig. 1C) and three-armed antispirals also emerged relatively often and randomly.

The center of an antispiral acts as a sink, where incoming waves disappear. To maintain an antispiral, new waves must emerge at the periphery, i.e., at the boundary between the basins (Fig. 1, A and B) belonging to two adjacent antispirals. The new waves then split and move apart, joining the two antispirals. This behavior apparently arises from the accelerating waves found in BZ-AOT microemulsions (*16*). Accelerating waves speed up when the distance between successive waves (wavelength) increases. When a wave between two basins splits into two new waves (2 and 3 in Fig. 1B) that merge into the neighboring antispirals, other waves (e.g., wave 1 in Fig. 1B) rush into the vacant area left by the split wave, along a direction perpendicular to the line joining the antispiral centers. When the wavelength is short, the velocity, v, is determined by the diffusion coefficient of water-soluble activator molecules, $HBrO_2$, i.e., by the diffusion coefficient of water droplets or clusters, $D_d = 10^{-7}$ to 10^{-8} cm^2/s, $v \sim (D_d)^{1/2}$. When the wavelength is long enough, v is determined instead by the diffusion coefficient of oil-soluble activator molecules, $BrO_2^{\bullet}$, which is about the same as the diffusion coefficient of small oil molecules, $D_{oil} \cong 10^{-5}$ cm^2/s, $v \sim (D_{oil})^{1/2}$. Thus, the velocity of accelerating waves may increase by an order of magnitude or more.

Accelerating waves also play an important role in the emergence of antispirals. A typical "initial" wave pattern is shown in Fig. 2A. Waves move toward the center of their arc (from bottom to top in Fig. 2). Each successive (lower) wave is longer than the preceding wave. Because of the free space in front of them, the ends of the lower wave move faster and therefore curl up around the ends of the preceding wave. This process is modulated by high-frequency phase waves originating from bulk oscillations. After the center of an antispiral forms (Fig. 2I), new traveling waves develop from phase waves and are added at the periphery of the evolving antispiral. Because $f_{AS} < f_{bulk}$, where f_{AS} and f_{bulk} are the frequencies of antispiral and bulk oscillations, respectively (point 3 in Table 1), the number of waves around the antispiral center increases. When the entire medium is occupied by antispirals and bulk oscillations are suppressed, new waves emerge at the Teflon gasket border and between antispirals.

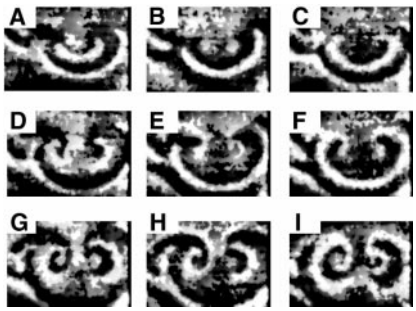

Fig. 2. Emergence of antispirals in BZ-AOT system for conditions as in Fig. 1B. Times (in seconds): (**A**) 1, (**B**) 17, (**C**) 37, (**D**) 113, (**E**) 132, (**F**) 146, (**G**) 225, (**H**) 242, and (**I**) 271. Frame size is 1.36 mm by 0.95 mm. Each set of three horizontal snapshots shows different stages of antispiral formation during one period (68 s) of bulk oscillations.

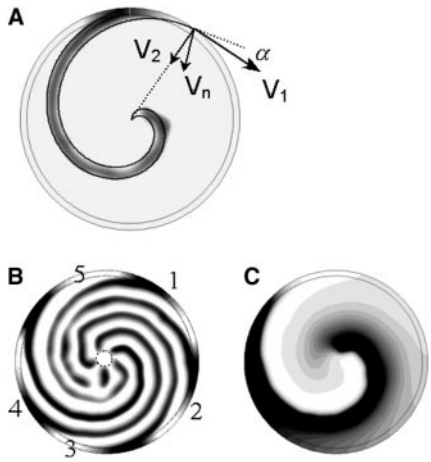

Fig. 3. Simulation of antispirals. Equations used are $dx/dt = [x - x^2 - fz(x - q)/(x + q)]/\varepsilon + D_x\Delta x$, $dz/dt = x - z + D_z\Delta z$, where $q = 1.5 \times 10^{-3}$, $f = 2.3$, $\varepsilon = 0.08$, $D_z = 0.04$, $D_x = 0.04$ on circle of radius $R_0 = 4.7$, and $D_x = 2$ on annulus of inner radius R_0 and outer radius $R_{out} = 5$. (**A**) The two bold spiral lines corresponding to Eq. 2 for $R_0 = 4.7$, $a = b = 1/(2\pi)$, and slightly different initial angles θ_0 are imposed on a spiral (x map) obtained in computer simulation [see (B)]. (**B**) x maps of antispirals separated in time by 1 s. (**C**) z map of antispiral corresponding to spiral 5 in (B).

Table 1. Comparative properties of inward antispirals and outward spirals.

Antispirals	Spirals
1. To a precision of several micrometers, the tip of an antispiral does not move. Simulations indicate the existence of a small core (see Fig. 3B).	1. All spirals have a core, around which the spiral tip rotates (*5*).
2. Antispirals have a pitch that increases with the distance from the center, R, and are described by Eq. 2, where $a \leq b$.	2. Spirals have a constant pitch and are well described as Archimedean: $R = \theta/2\pi$ (*1*).
3. $f_{AS} < f_{bulk}$.	3. $f_S > f_{bulk}$, where f_S is the frequency of spiral oscillations (*25, 26*).
4. Waves (arms) of a single antispiral can break, collide, and merge far from the spiral's center.	4. Waves belonging to a stable spiral never collide with one another (*27*).
5. New waves emerge at the boundary between two adjacent antispirals.	5. Waves from two neighboring spirals annihilate at the boundary between them (*1*).
6. Antispiral waves move toward the center of their arc. The curvature increases as the waves propagate.	6. Spiral waves move out from the center of their arc. Wave propagation leads to a decrease in curvature (*25*).

If we draw a circle whose center coincides with the center of an antispiral and whose radius is equal to two to three pitches, an "impulse" or the "open end of a spiral" (actually, a piece of a wave at the intersection between an incoming wave and the circle) will appear to circulate around the border of the circle with velocity $V_1 = V_n/\sin\alpha$, where α is the angle between the radius vector to the cross point and the incoming wave with normal velocity V_n (see Fig. 3A). We use this notion of a virtual impulse to simulate antispirals on a ring for a two-variable model of the excitable BZ reaction (*14*). First, we create a high-speed rotating impulse with velocity V_1 on a narrow annular ring with inner and outer radii R_0 and R_{out}, respectively (R_0 is slightly smaller then R_{out}; see Fig. 3). We do this by increasing the initial concentration of activator (x) above the threshold of excitation on a small segment of the annular ring, while the initial concentration of catalyst (z) is slightly increased on a narrow neighboring segment of the circle with radius R_{out}. If the initial concentrations are equal to their steady-state values everywhere else, the impulse propagates away from the direction of the elevated catalyst concentration (clockwise). This impulse produces a wave on the circle of radius R_0 that propagates toward the center with velocity V_2. The values V_1 and V_2 are controlled by the (different) diffusion coefficients of the activator species on the annular ring and on the circle.

Antispirals are obtained for the case when $V_1/V_2 > 2\pi$ and the refractory period (time necessary for the medium to recover and sustain a new impulse after the previous one passes) is less than $2\pi R_0/V_1$ (see Fig. 3, B and C). Near the antispiral core, sharp angles between neighboring fragments of the spiral wave may emerge when the curvature is very large (waves 1 and 3 in Fig. 3B), leading to an intermittent break in the wave (wave 2 in Fig. 3B). We also observed such behavior in our experiments. Obtaining antispirals with this simple two-variable model implies that if an antispiral is somehow created, no special

wave properties (such as extremely different diffusion coefficients for the activator species) are necessary to sustain it in the area close to the antispiral core. However, generation of new waves between the basins of two adjacent antispirals does require special properties (*16*).

From the simple relations $R = R_0 - V_2 t$ and $\theta - \theta_0 = V_1 t/(2\pi R_0)$, where θ is the angular position measured in radians, θ_0 is an initial angle, and R is the distance from the center ($\theta - \theta_0 > 0$, $R > 0$), the equation for an inwardly rotating spiral can be deduced. For simplicity, we assume that, as a result of dispersion relations and curvature effects, V_2 is linearly dependent on the radius, so that $V_2 = V_c + R(V_0 - V_c)/R_0$, where V_c and V_0 are the velocities at the center ($R = 0$) and at $R = R_0$, respectively. Combining these three relations to eliminate the time, we obtain

$$R = R_0[1 - a(\theta - \theta_0)]/[1 + (b - a)(\theta - \theta_0)] \quad (2)$$

where $a = V_c/V_1$ and $b = V_0/V_1$. Comparison between Eq. 2 and a simulated spiral for the case $a = b$ is shown in Fig. 3A. In Table 1, we compare the characteristic features of spirals and antispirals.

Examples of inwardly rotating spirals may be found in hydrodynamics and in Newtonian mechanics. Water funnels and the trajectory of a rotating body attracted by a large mass are simple examples of inward spirals. Inwardly propagating, but nonrotating, spiral cracks were obtained recently by drying an aqueous suspension of precipitate (*23*). Spirals may be classified according to whether they grow from the center or from the periphery. In outwardly rotating spirals, such as those in the aqueous BZ reaction, the point of growth is the center, the tip of the spiral. The direction of spiral propagation provides a second criterion for spiral classification. In spiral cracks, the growing point is also the tip of the spiral, but in this case the spiral curls up to and stops at the center. Peripheral spiral growth occurs, for example, in mollusc shells (nonrotating three-dimensional spirals) and in our case of rotating two-dimensional antispirals. In marine shells, the lime arms of the spiral neither move nor disappear, and therefore the spiral shell grows out from the center. In antispirals, the waves propagate in toward the center, and the peripheral growth is compensated by wave annihilation in the core. Thus, although antispirals may appear to contradict our usual notions about spiral waves, they actually fit neatly into the family of spiral behaviors. What is remarkable in the present system is how easily the type of spiral can be changed by a small variation in the structure of the microemulsion or in the chemical composition.

Two examples are known of inwardly propagating circular waves in related systems. Under some conditions, aggregating *D. discoideum* amoebae generate patterns that look like inward concentric waves, although it is the outwardly moving waves of cAMP that drive the system (*13*). A second example is found in the ring-shaped pulsating waves of inhibition (reducing waves) seen by Marek *et al.* (*24*) in the BZ reaction. It seems likely that antispirals occur in living heterogeneous systems, such as brain tissue, heart muscle, or colonies of microorganisms, where spiral behavior has already been observed.

References and Notes

1. A. T. Winfree, *Science* **175**, 634 (1972).
2. A. N. Zaikin, A. M. Zhabotinsky, *Nature* **225**, 535 (1970).
3. K. Agladze, V. I. Krinsky, *Nature* **296**, 424 (1982).
4. K. Agladze, J. P. Keener, S. C. Müller, A. Panfilov, *Science* **264**, 1746 (1994).
5. S. C. Müller, T. Plesser, B. Hess, *Science* **230**, 661 (1985).
6. V. Pérez- Muñuzuri, R. Aliev, B. Vasiev, V. Pérez-Villar, V. I. Krinsky, *Nature* **353**, 740 (1991).
7. G. Ertl, *Science* **254**, 1750 (1991).
8. J. M. Davidenko, A. V. Pertsov, R. Salomonsz, W. Baxter, J. Jalife, *Nature* **355**, 349 (1992).
9. A. T. Winfree, *Science* **266**, 1003 (1994).
10. F. X. Witkowski *et al.*, *Nature* **392**, 78 (1998).
11. M. P. Hassell, H. N. Comins, R. M. May, *Nature* **353**, 255 (1991).
12. J. Lechleiter, S. Girard, E. Peralta, D. Clapham, *Science* **252**, 123 (1991).
13. K. J. Lee, E. C. Cox, R. E. Goldstein, *Phys. Rev. Lett.* **76**, 1174 (1996).
14. J. P. Keener, J. J. Tyson, *Physica D* **21**, 307 (1986).
15. V. S. Zykov, *Biophysics* **25**, 906 (1980).
16. V. K. Vanag, I. R. Epstein, *Phys. Rev. Lett.*, in press.
17. C. T. Hamik, N. Manz, O. Steinbock, *J. Phys. Chem. A* **105**, 6144 (2001).
18. V. I. Zarnitsina, F. I. Ataullakhanov, A. I. Lobanov, O. L. Morozova, *Chaos* **11**, 57 (2001).
19. D. Balasubramanian, G. A. Rodley, *J. Phys. Chem.* **92**, 5995 (1988).
20. V. K. Vanag, I. Hanazaki, *J. Phys. Chem.* **99**, 6944 (1995).
21. T. K. De, A. Maitra, *Adv. Colloid Interface Sci.* **59**, 95 (1995).
22. E. O. Budrene, H. C. Berg, *Nature* **376**, 49 (1995).
23. K.-T. Leung, L. Józsa, M. Ravasz, Z. Néda, *Nature* **410**, 166 (2001).
24. M. Marek, P. Kaštánek, S. C. Müller, *J. Phys. Chem.* **98**, 7452 (1994).
25. M. Gerhardt, H. Schuster, J. J. Tyson, *Science* **247**, 1563 (1990).
26. K. J. Lee, *Phys. Rev. Lett.* **79**, 2907 (1997).
27. Q. Ouyang, J.-M. Flesselles, *Nature* **379**, 143 (1996).

28. We thank A. M. Zhabotinsky for helpful discussions. This work was supported by the Chemistry Division of the NSF.

6 July 2001; accepted 24 September 2001

Observation of Charge Transport by Negatively Charged Excitons

Daniele Sanvitto,[1,2] Fabio Pulizzi,[3] Andrew J. Shields,[1]* Peter C. M. Christianen,[3] Stuart N. Holmes,[1] Michelle Y. Simmons,[2]† David A. Ritchie,[2] Jan C. Maan,[3] Michael Pepper[1,2]

We report transport of electron-hole complexes in semiconductor quantum wells under applied electric fields. Negatively charged excitons (X^-), created by laser excitation of a high electron mobility transistor, are observed to drift upon applying a voltage between the source and drain. In contrast, neutral excitons do not drift under similar conditions. The X^- mobility is found to be as high as 6.5×10^4 cm^2 V^{-1} s^{-1}. The results demonstrate that X^- exists as a free particle in the best-quality samples and suggest that light emission from opto-electronic devices can be manipulated through exciton drift under applied electric fields.

The exciton, the bound state resulting from the Coulomb attraction of an optically excited electron-hole pair, is often described as the semiconductor analog of the hydrogen atom. In 1958, Lampert (*1*) speculated on the existence of a class of mobile excitons, the analogs of the negative hydrogen ion (H^-) and positive hydrogen molecule (H_2^+) (*2*). However, because the binding energy of the second electron to the electron-hole pair is quite small, unambiguous observation (*3*) of a spectral line due to the negatively charged exciton (which is also called a trion) did not follow until the advent of high-quality remotely doped quantum well structures, in which the trion binding energy is substantially increased (*4*). This occurs at a very low excess electron density, at which each photoexcited electron-hole pair interacts with and

[1]Toshiba Research Europe Limited, Cambridge Research Laboratory, 260 Cambridge Science Park, Milton Road, Cambridge, CB4 0WE, UK. [2]Cavendish Laboratory, University of Cambridge, Madingley Road, Cambridge, CB3 0HE, UK. [3]High Field Magnet Laboratory, University of Nijmegen, Toernooiveld 1, 6525 ED Nijmegen, Netherlands.

*To whom correspondence should be addressed. E-mail: andrew.shields@crl.toshiba.co.uk

†Present address: School of Physics, University of New South Wales, Sydney 2052, Australia.